Low Dimensional Approximations to Ferroelastic Dynamics and Hysteretic Behavior Due to Phase Transformations

Linxiang X. Wang
Institute of Mechatronic Engineering,
Hangzhou Dianzi University,
Hangzhou 310037, China;
MCI,
Faculty of Science and Engineering,
University of Southern Denmark,
Sonderborg DK-6400, Denmark

Roderick V. N. Melnik[1]
M^{2}NeT Lab,
Wilfrid Laurier University,
75 University Avenue West,
Waterloo, ON, N2L 3C5, Canada
e-mail: rmelnik@wlu.ca

In this paper, a low dimensional model is constructed to approximate the nonlinear ferroelastic dynamics involving mechanically and thermally-induced martensite transformations. The dynamics of the first order martensite transformation is first modeled by a set of nonlinear coupled partial differential equations (PDEs), which is obtained by using the modified Ginzburg–Landau theory. The Chebyshev collocation method is employed for the numerical analysis of the PDE model. An extended proper orthogonal decomposition is then carried out to construct a set of empirical orthogonal eigenmodes of the dynamics, with which system characteristics can be optimally approximated (in a specified sense) within a range of different temperatures and under various mechanical and thermal loadings. The performance of the low dimensional model is analyzed numerically. Results on the dynamics involving mechanically and thermally-induced phase transformations and the hysteresis effects induced by such transformations are presented. [DOI: 10.1115/1.4000381]

Keywords: ferroelastic dynamics, phase transformations, coupled dynamic thermoelasticity, optimal approximation, extended proper orthogonal decomposition, Galerkin projection, multiphase solids, smart materials and structures, shape memory alloys, metastable phases, low dimensional models, multiscale problems, model reduction

1 Introduction

Due to their unique properties, the ferroelastic materials have attracted intensive research efforts from engineers, physicists, mathematicians, and control theorists. Ferroelastic materials can sense and respond or actuate on the mechanical or thermal loadings. When thermal or mechanical loadings are applied, the material can intrinsically convert the energy between the mechanical and thermal fields, and produce thermal and mechanical responses correspondingly. By tuning the loadings, the dynamical behavior of the material then can be adjusted or controlled according to the requirement of a specific application [1]. In many applications, it controls such a behavior in some systematic manner that is really the focus of much of the attention of the ferroelastic/ferroelectric community [2–4]. In addition, in many applications the optimal design of smart structures and their components are also desirable. For all these applications, the development of a suitable mathematical model describing the full dynamics of the material, and such that it is suitable for control and optimization purposes, becomes essential.

Most of the currently existing mathematical models for dynamic behaviors of smart materials are given by partial differential equations (PDEs) with couplings between various, often nonlinear, physical fields [2,5–13]. For ferroelastic materials involving the first order martensite phase transformation, the mathematical models can be formulated by coupling the thermal and mechanical fields [14–26]. Due to the nonlinear nature of phase transformations, the dynamics of the mechanical field is strongly nonlinear and amplified by nonlinear coupling with the thermal field. Since the dynamics of ferroelastic materials can be described by a system of nonlinear coupled PDEs, we usually have to deal with an infinite dimensional space [27,28]. However, for control and design optimization purpose, an infinite dimensional model is difficult to deal with [15,20,29,30], especially when the system is nonlinear.

One of the usual ways to cope with this difficulty is to discretize the PDE-based model spatially and convert it into a set of ordinary differential equations (ODEs) using the method of lines [19]. Because of the coupling between the multiphysics fields and system nonlinearity, the number of nodes for the spatial discretization might have to be chosen large. Another potential difficulty is the stiffness of the resultant ODE system. As a result, we have to face a number of challenges while controlling engineering systems described by time-dependent PDEs, even in relatively simple linear cases (e.g., Refs. [29–34]).

For engineering applications, model reduction methods are employed to reduce the dimension and complexity of the resultant system so that the original PDE systems could be approximated by lower dimensional ODE systems or systems of differential-algebraic equations [8,14,35–38]. Proper orthogonal decomposition (POD) method is a very efficient practical tool for this purpose if a collection of system states is available. Among other application areas, this method has been successfully applied to active control of fluid flow problems [39,40]. More recently, the POD method has also been successfully applied to modeling the dynamics of a shape memory alloys rod [38], as well as the dynamics of patches involving mechanically induced first order transformations [4], albeit at a specific temperature range.

In employing POD for the analysis of the dynamics of ferroelastic structures in Refs. [4,38], the low dimensional model could only approximate the dynamics with a certain initial temperature. Furthermore, only the mechanically induced phase transformations could be approximated. This limitation is due to the fact that the POD method normally can treat only one parameter. For the ferroelastic materials, it is important that the mathematical model is capable of modeling the dynamics involving both me-

[1]Corresponding author.

Contributed by the Applied Mechanics of ASME for publication in the JOURNAL OF APPLIED MECHANICS. Manuscript received January 18, 2006; final manuscript received August 3, 2009; published online February 24, 2010. Assoc. Editor: Igor Mezic.

chanically and thermally-induced phase transformations, within the entire range of considered temperatures. Indeed, ferroelastic materials have very different behaviors within different temperature regimes [28,36,41]. At high temperatures, only austenite (A) is stable, and the material behaves in a superelastic manner with no pronounced hysteresis effects (due to the absence of phase transformations at high temperature). At low temperatures, only martensite variants (e.g., $M+$ and $M-$ in one dimension) are stable, and transformations can be induced mechanically between $M+$ and $M-$ or thermally between A and $M+$ ($M-$). In the latter case, the materials behave in a pseudo-elastic (rubberlike) manner. If the material temperature is close to the transformation reference temperature, both austenite and martensite can co-exist, and mechanical loadings might induce phase transformations between A, $M+$, and $M-$. For a given phase transformation, there is always a hysteresis loop associated with it.

In this paper, the POD method is employed and extended to construct the low dimensional model for the dynamics of ferroelastic materials. The developed methodology is capable of capturing different characteristics of these materials' behavior at any considered temperatures. The idea is to construct a set of orthogonal eigenmodes using collections of system states. The eigenmode series is then truncated, and the dynamics of the system is orthogonally projected onto the subspace spanned by the truncated eigenmode series. This projection yields the low dimensional model we are looking for. The eigenmodes are constructed using the extended POD method. The performance of the low dimensional model is demonstrated by simulating both thermal and mechanical phase-transformation-induced hysteresis. It is shown that the empirical low dimensional model captures the main characteristic behavior of the material under all applicable temperature ranges.

2 Coupled Dynamic Thermoelasticity Models and Numerical Simulation

Starting from the Danilovskaya problem [42], first formulated in the early 1950s, the dynamic theory of thermoelasticity has grown into a mature subject with a wide range of important applications in sciences and engineering. In the case of linear dynamic thermoelasticity, a number of efficient numerical techniques have been developed and analyzed [21,43], including extensions to thermo-electroelasticity [7,9] and hyperbolic dynamic thermoelasticity [44,45] and their applications to modeling shape memory alloys and other materials in smart materials and structures technology [14,36]. New technologies bring new challenges to this rapidly evolving field and applications of dynamic thermoelasticity in such areas as the analysis of thermal deformations induced by ultrashort lasers and thermal processing of nanophase materials led to further focus on the development of numerical procedures [46–48]. These new developments led to the possibility of accounting for such complex effects as the hot-electron blast effect in momentum transfer, coupling between lattice temperature, and strain rate and others. Coupled thermoelastic problems may become increasingly important in modeling inhomogeneous media in the context of light-solid interactions and in related problems of nanotechnology [33,49–54].

Higher order nonlinearities (such as quintic) that are typical in modeling phase transformations in ferroelastic and ferroelectric materials [24,36,55] and their multiscale nature [10] bring numerical challenges of coupled multiphysics problems at a new level, where some such models are among the greatest computational challenges in mathematical modeling [8]. An increasing number of engineering applications leads to a growing interest to the analysis of the dynamics of ferroelastic materials involving the first order phase transformations. Such an analysis can be carried out with mathematical models based on the modified Ginzburg–Landau theory and a number of numerical experiments demonstrating the effectiveness of this approach have been reported in the literature, particularly in one-dimensional (1D) cases [28,35,36,56].

In the context of phase transformations in ferroelastic materials, the developed numerical methodologies include conservative finite difference schemes [27,28], finite element approximations for nonequilibrium thermodynamics based models for thin films [18,22], and for more general three-dimensional (3D) multivariant situations [16,20,23,57], the method of lines [19], finite volume methods [58,59], and hybrid optimization methodologies [25]. Many of the proposed methodologies are based on the original reduction in the PDE model to a system of differential-algebraic equations, first proposed in Ref. [14] and developed further in Refs. [8,35–38], along with several low dimensional models. Earlier attempts to apply pseudospectral (collocation) methodologies can be found in Refs. [60,61]. This line of research is developed further in Secs. 3–6 by supplementing it with the extended proper orthogonal decomposition technique.

2.1 Model for Martensite Phase Transformations in Ferroelastic Materials. As discussed above, time-dependent mathematical models describing coupled thermomechanical wave interactions keep the key to many different applications [12,27,43–45,47,48]. To account for the first order phase transformations in ferroelastic materials, such as shape memory alloys, these models of coupled dynamic thermoelasticity must account for a nonconvex highly nonlinear character of the associated free energy function. We start with the following 1D mathematical model [28,35,36,38]:

$$\rho\frac{\partial^2 u}{\partial t^2}=\frac{\partial}{\partial x}\left(k_1(\theta-\theta_1)\frac{\partial u}{\partial x}-k_2\left(\frac{\partial u}{\partial x}\right)^3+k_3\left(\frac{\partial u}{\partial x}\right)^5\right)+\nu\frac{\partial}{\partial t}\frac{\partial^2 u}{\partial x^2}-\delta\frac{\partial^4 u}{\partial x^4}+F$$

$$c_v\frac{\partial\theta}{\partial t}=k\frac{\partial^2\theta}{\partial x^2}+k_1\theta\frac{\partial u}{\partial x}\frac{\partial v}{\partial x}+G \tag{1}$$

where u is displacement, θ is temperature, ρ is density, k_1, k_2, k_3, c_v, ν, δ, and k are normalized material-specific constants, θ_1 is the reference temperature for 1D martensitic transformations, and F and G are distributed mechanical and thermal loadings. The interested reader can find efficient numerical procedures for reducing systematically the general 3D model to models such as Eq. (1) in Refs. [36,37].

Although this is only a 1D model for the nonlinear dynamics of ferroelastic materials, it presents a number of challenges in its analysis and numerical implementation due to the coupling between thermal and elastic fields and strong nonlinearities. Furthermore, the inclusion of thermal and mechanical hystereses and the first order martensitic transformations into the model gives additional difficulties. First, we rewrite the above system for numerical convenience as follows [28,35]:

$$c_v\frac{\partial\theta}{\partial t}=k\frac{\partial^2\theta}{\partial x^2}+k_1\theta\epsilon\frac{\partial v}{\partial x}+G,\quad \frac{\partial\epsilon}{\partial t}=\frac{\partial v}{\partial x}$$

$$\rho\frac{\partial v}{\partial t}=\frac{\partial}{\partial x}(k_1(\theta-\theta_1)\epsilon-k_2\epsilon^3+k_3\epsilon^5)+\nu\frac{\partial}{\partial t}\frac{\partial^2 u}{\partial x^2}-\delta\frac{\partial^3\epsilon}{\partial x^3}+F \tag{2}$$

where $\epsilon=\partial u/\partial x$ is the strain, and $v=\partial u/\partial t$ is the velocity.

We note the appearance of the Rayleigh dissipation term $\nu(\partial/\partial t)(\partial^2 u/\partial x^2)$ in models (1) and (2). This term is added in order to account for the internal friction, accompanying wave propagations, and phase transformations, which will be translated into viscous effects at macroscale (see details in Ref. [24] and references therein). From a numerical point of view, it allows us to avoid nonphysical oscillations in the solution. Such internal friction/viscosity terms play an important role in modeling physi-

cal, biological, and engineering systems [11,24,61,62].

The above model for the dynamics of the first order phase transformation has been constructed on the basis of the Landau free energy function, which allows one to characterize different stable phases at different temperatures [28,35,38]

$$W_L = \frac{k_1}{2}(\theta - \theta_1)\epsilon^2 - \frac{k_2}{4}\epsilon^4 + \frac{k_3}{6}\epsilon^6 \tag{3}$$

Using W_L, from thermodynamics equilibrium conditions for the considered material, the constitutive law for the mechanical field is then obtained as

$$\sigma = k_1(\theta - \theta_1)\epsilon - k_2\epsilon^3 + k_3\epsilon^5 \tag{4}$$

where σ is the stress.

In what follows, we consider the following boundary conditions [56]:

$$\frac{\partial \theta}{\partial x} = 0, \quad \frac{\partial \varepsilon}{\partial x} = 0, \quad v = 0, \quad \text{at } x = 0, L \tag{5}$$

2.2 Chebyshev Collocation Methods. The model presented in Sec. 2.1 is not amenable to analytical solution, and hence one has to resort to numerical methods as it is often the case for other problems of coupled field theory applied in modeling smart other functional materials and structures and complex systems [5,6,13,63–69]. Many efficient numerical methodologies for time-dependent PDEs are based on an assumption that the solution can be approximated by the following linear combination:

$$f^N(x,t) = \sum_{i=0}^{N} f_i(t)\phi_i(x) \tag{6}$$

where $\phi_i(x)$ is the basis functions (trial functions), and $f_i(t)$ is the expansion coefficients. $f^N(x,t)$ stands for the Nth order approximation to the solutions we are looking for.

The intrinsic feature of spectral-type methodologies is that all the basis functions are assumed differentiable in the entire computational domain with derivatives given as

$$\frac{\partial f(x,t)}{\partial x} = \sum_{i=0}^{N} f_i(t)\frac{d\phi_i(x)}{dx}$$

$$\frac{\partial f(x,t)}{\partial t} = \sum_{i=0}^{N} \phi_i(x)\frac{df_i(t)}{dt} \tag{7}$$

and similarly for higher order derivatives if they are present.

For the sake of convenience, the governing equations are rewritten in the form of evolution operator equation

$$\frac{d\mathcal{U}}{dt} = \mathcal{M}(\mathcal{U}) \tag{8}$$

where $\mathcal{U}$ is the solution and $\mathcal{M}(\mathcal{U})$ is an operator, which contains all the spatial derivatives of $\mathcal{U}$. In general, the approximation given by Eqs. (6) and (7) will not satisfy Eq. (8), i.e., the residual

$$\mathcal{R} = \frac{d\mathcal{U}^N}{dt} - \mathcal{M}(\mathcal{U}^N) \tag{9}$$

will not vanish everywhere. To determine all the expansion coefficients, the Galerkin method requires the following condition to be satisfied:

$$\int_0^L \left(\frac{d\mathcal{U}^N}{dt} - \mathcal{M}(\mathcal{U}^N)\right)\psi_i(x)dx = 0, \tag{10}$$

where $\psi_i(x)$ are the test functions.

In the Chebyshev collocation methods the trial functions are chosen to satisfy the following conditions:

$$\phi_i(x_j) = \begin{cases} 1, & i = j \\ 0, & i \neq j \end{cases} \tag{11}$$

and the test functions are chosen as

$$\psi_i(x) = \delta(x_i) = \begin{cases} 1, & x = x_i \\ 0, & x \neq x_i \end{cases} \tag{12}$$

where $\{x_i\}$ is a set of chosen discretization points in the computational domain. For the Chebyshev approximation, it is chosen as follows:

$$x_i = L\left(1 - \cos\left(\frac{\pi i}{N}\right)\right)/2, \quad i = 0,1,\ldots,N \tag{13}$$

where L is the length of the considered ferroelastic rod.

Following the standard procedure (e.g., Ref. [70]), Eq. (7) can be written in a matrix form as

$$\mathbf{U}_x = \mathbf{D}\mathbf{U} \tag{14}$$

By substituting corresponding approximations of the spatial derivatives, the PDE-based model is converted into a set of differential-algebraic equations (DAEs). The idea of a reduction in the original PDE model to a system of DAEs was first proposed in Ref. [14], followed by a subsequent development of low dimensional models based on the center manifold technique [36,37]. The application of an efficient time integrator can finally solve the problem in a way similar to what was discussed earlier [4,28,35,38]. The described methodology allows us to determine the temperature, stress, strain, and displacement of the material at any point of the computational domain at any time. Then, the resultant data can be used for the POD analysis.

3 POD Method for System With One Parameter

3.1 Orthonormal Basis. If the procedure described in Sec. 2 is employed and various collections of system states are obtained, then the eigenmode series for the approximation to the system dynamics can be constructed using the extended POD method. To do so, we start the discussion from the regular POD analysis with one parameter.

For convenience, the system dynamics given by Eq. (8) can be regarded as autonomous where $\mathcal{U}(x,t)$ is the function vector we are solving for (consisting of ϵ, v, and θ). The solution depends continuously on the spatial position in a given domain Ω. Operator $\mathcal{M}$ in this case is a vector consisting of nonlinear functions of $\mathcal{U}$ and their first and second order derivatives.

The POD is concerned with the possibility of finding a set of orthonormal basis functions $\phi = \{\phi_j(x), j = 1,\ldots,P\}$, which is optimal in the sense that the P dimensional approximation

$$\mathcal{U}_P(x,t) = \sum_{i=1}^{P} a_i(t)\phi_i(x) \tag{15}$$

gives the best least-squares approximation to the function $\mathcal{U}(x,t)$ among all such P dimensional approximations [39,40,71]. Here a_i is the general (time-dependent) Fourier coefficient associated with $\{\phi_k\}$. In other words, the POD idea in this context is to choose the basis functions $\{\phi_k\}$ to maximize the mean projection of the function $\mathcal{U}(x,t)$ on $\{\phi_k\}$

$$\max_{\phi \in L_2(\Omega)} \frac{E(|\langle \mathcal{U}, \phi \rangle|^2)}{\|\phi\|^2} \tag{16}$$

where $E(\cdot)$ denotes the mean value functional, and $\langle \cdot \rangle$ is the inner product [39,40]. Finally, the maximization problem leads to the following eigenvalue problem:

$$\int_{\Omega} E(\mathcal{U}(x)\mathcal{U}(x'))\phi(x')dx' = \lambda\phi(x) \tag{17}$$

with kernel $\mathcal{K}=E(\mathcal{U}(x)\mathcal{U}(x'))$ being the autocovariance function of the two points x and x'.

By solving the above eigenvalue problems, a series of eigenvalues and eigenfunctions (eigenmodes) can be obtained (note that in some cases, this problem involves nontrivial issues due to a highly oscillatory character of the solution, which can be overcome with techniques developed earlier [72–76]). If we arrange the eigenvalue pairs in a monotonically decreasing way, the lower dimensional approximation of the solution $\mathcal{U}$ can be easily obtained by just keeping the first few largest eigenvalues and their associated eigenfunctions, and the dynamics can then be orthogonally projected onto the subspace spanned by the few kept eigenfunctions. The number of eigenfunctions should be determined by compromising between the dimension of the resultant system and the approximation accuracy [39,77].

The eigenfunctions obtained from the above eigenvalue problem are orthonormal, which gives us the following relations:

$$\langle\phi_i,\phi_j\rangle = \int_{\Omega} \phi_i\phi_j dx = \begin{cases} 1 & \text{if } i=j \\ 0 & \text{if } i\neq j \end{cases} \tag{18}$$

In the discrete case, the eigenfunctions will be replaced by eigenvectors and the orthonormal relation can be written as

$$\langle\phi_i,\phi_j\rangle = \phi_i^T\phi_j = \begin{cases} 1 & \text{if } i=j \\ 0 & \text{if } i\neq j \end{cases} \tag{19}$$

where superscript T stands for transpose. The general Fourier coefficients in this case could be calculated as

$$a_k = \langle U,\phi_k\rangle \tag{20}$$

3.2 Galerkin Projection. Having obtained optimal basis functions for the dynamical system, its lower dimensional approximation can be obtained by projecting the full system orthogonally onto the subspace spanned by the chosen basis functions. The model reduction can be achieved due to the fact that a much smaller number of basis functions is needed for the approximation of the full system, provided the chosen basis functions are optimal in a sense specified above.

Let us denote the projection operator by P_r and by P_r^T, its transpose. Then, a low dimensional system on the chosen subspace S can be constructed using the following rule: For any point $\boldsymbol{Z}\in S$, compute the vector field $\boldsymbol{M}(t,P_r^T\boldsymbol{Z})$ and take the projection $P_r\boldsymbol{M}(t,P_r^T\boldsymbol{Z})$ onto the subspace S, it should be equal to $\dot{\boldsymbol{Z}}$. This can be formally formulated as

$$\frac{d}{dt}\boldsymbol{Z} = P_r\boldsymbol{M}(t,P_r^T\boldsymbol{Z}) \tag{21}$$

where the vector field $\boldsymbol{M}$ is the vector $\boldsymbol{M}$ in the dynamical system (or its discretization in the spatial domain).

For the modeling of hysteretic dynamics in ferroelastic materials, the low dimensional ODE model given by Eq. (21) is expected to be capable of capturing both phase transitions and thermomechanical coupling between the thermal and mechanical fields. Phase transitions can be investigated qualitatively by analyzing the stability of equilibria and jumping of system states from one stable branch to another, which corresponds to the phase transition process. In the current context, the low order ODE model given by Eq. (21) is based on empirical eigenmodes, which are all specified in a purely numerical (implicit) way as analytical expressions are not available. For this reason, it is not practical (and far from trivial) to carry out a stability analysis for each equilibria and investigate transitions of system states, in particular, in view of the complexity of the underlying problem. The results in this direction are available only for a few special cases [78–81]. Using another approach, the dynamics given by the PDE model is approximated by a lower dimensional model in the context of center manifold approximation, by which stability analysis of equilibria, as well as hysteresis induced by jumping of system states among stable branches, has also been carried out in Ref. [37].

Certainly, the approximation will introduce some error, which can be defined as follows:

$$r = \boldsymbol{X} - P_r^T\boldsymbol{Z} \tag{22}$$

In order to minimize the error in the approximation with the given basis, we require that the error function of the approximation should be orthogonal to all the basis functions

$$\langle r,\phi_k\rangle = \int_{\Omega} r(x)\phi(x)dx = 0 \tag{23}$$

It is easy to check that the low dimensional system given by Eq. (21) satisfies this condition, if the orthogonality of the basis functions is used.

If the low dimensional model is constructed to approximate the full system dynamics with only one of its parameters varied, the above mentioned POD method and Galerkin projection is able to give a satisfactory approximation. When the system dynamics to be approximated is influenced by more than one of such parameters, and the characteristics of the dynamics are very different for different parameter values, the above mention POD method will fail in constructing a set of orthogonal eigenmodes for the optimal approximation of the system dynamics. A new approach should be employed to construct the basis functions.

4 Extended POD Method

For the current problem, the phase transformation can take place at different temperatures by either mechanical or thermal stimulations. There may be no phase transformation if the temperature is sufficiently high. In order to model the dynamics of the ferroelastic material correctly, the empirical eigenfunctions have to take into account the temperature influence.

There are different approaches to construct the eigenmodes for the dynamics of a system depending on more than one parameter. One is the interpolation of the eigenmodes associated with different parameters (Ref. [82] and references therein), by which one implicitly assumes that characteristics of the system dynamics vary smoothly when parameter values are changed. Here we follow another approach, which is called the extended POD method (Ref. [83] and references therein). As follows from Eq. (2), it is clear that the mechanical field is influenced by the temperature through one of its coefficients. Hence, we can choose a few representative temperature values to do the analysis. We choose three initial temperature values for which the system has only a martensite phase (low temperature θ_1), metastable austenite, and martensite phases (medium temperature θ_2), or only an austenite phase (high temperature θ_3), respectively.

Let us denote the collection of snapshots with initial temperatures θ_1 as $\boldsymbol{U}_1$. We will refer to it as one block of the overall collection. Similarly, we call block $\boldsymbol{U}_2$ with θ_2, and block $\boldsymbol{U}_3$ with θ_3. When the system dynamics has very different behaviors at different temperatures, this means that the characteristics embedded in the blocks should be very different. If one employs the POD method directly to all the overall snapshots $\boldsymbol{U}=[\boldsymbol{U}_1,\boldsymbol{U}_2,\boldsymbol{U}_3]$ by putting all snapshots together, the characteristics of different blocks will be mixed and dispersed with each other. Alternatively, one has to include the eigenmodes from all the blocks, which will certainly increase the number of overall basis functions and, furthermore, will lead to the loss of the basis functions orthogonality.

In order to deal with this difficulty, the extended POD method is employed here to construct the eigenmodes using the snapshots collected in all the blocks. The strategy we employ in the context of the extended POD can be explained as follows [83]. First, the

POD analysis is applied to the block $\boldsymbol{U}_1$, it will give us a set of eigenmodes for system dynamics associated with initial temperature θ_1

$$\boldsymbol{U}_1 = \sum_{i=1}^{N_1} C_1^i \phi_1^i = \phi_1 \boldsymbol{C}_1 \tag{24}$$

where N_1 is the number of basis function used for the construction of the subspace for approximation, ϕ_1 is the matrix that consists of the eigenmodes ϕ_1^i, $i=1,2,\ldots,N_1$ as its columns, and $\boldsymbol{C}_1$ is the vector that consists of all the general Fourier coefficients.

For the second block, there is no need to extract those characteristics included in ϕ_1 from the first block, it will be more effective if the characteristics embedded in ϕ_1 are removed from block $\boldsymbol{U}_2$ before the POD analysis. To do so, the snapshots in $\boldsymbol{U}_2$ are first projected onto the subspace spanning by ϕ_1, the general Fourier coefficients for the projections are $\phi_1^T \boldsymbol{U}_2$. The complementary subspace is as follows:

$$\boldsymbol{W}_2 = \boldsymbol{U}_2 - \phi_1 \phi_1^T \boldsymbol{U}_2 \tag{25}$$

in which the term $\phi_1 \phi_1^T \boldsymbol{U}_2$ gives orthogonal projection of U_2 onto ϕ_1. It is clear that $\boldsymbol{W}_2$ is orthogonal to ϕ_1 because the projection is orthogonal. Now the complementary subspace $\boldsymbol{W}_2$ includes no characteristics embedded in ϕ_1 and can be analyzed using the POD methods, by which the eigenmodes for $\boldsymbol{W}_2$ can be obtained as

$$\boldsymbol{W}_2 = \sum_{i=1}^{N_2} C_2^i \phi_2^i = \phi_2 \boldsymbol{C}_2 \tag{26}$$

where N_2 is the number of eigenmodes for approximation to $\boldsymbol{W}_2$, and ϕ_2 is orthogonal to ϕ_1.

By carrying out the POD analysis, as described above, the approximation to the second block U_2 can be formulated as

$$\boldsymbol{U}_2 = \phi_1 \phi_1^T \boldsymbol{U}_2 + \phi_2 \boldsymbol{C}_2 \tag{27}$$

which is obvious from Eqs. (25) and (26)

The above treatment can be explained as follows. For the considered system, if the characteristics of the dynamics embedded into two blocks of snapshots U_1 and U_1 are essentially the same, the subspace ϕ_1 will also be able to give a very good approximation to U_2, which means that $\boldsymbol{W}_2$ will be zero, so that the subspace spanned by ϕ_2 will be empty. This is just the same as the regular POD analysis for a single block of snapshots [83]. For the current problems, it is obviously not true, as we mentioned earlier, because the system dynamics is very different within different temperature ranges. While at another extremal point, blocks $\boldsymbol{U}_1$ and $\boldsymbol{U}_2$ are totally independent (no similarity at all), the orthogonal projection of $\boldsymbol{U}_2$ onto ϕ_1 will give all coefficients zero, and $\boldsymbol{W}_2$ is the same as $\boldsymbol{U}_2$. Normally, this would not happen because there must be some similarities between the blocks of snapshots, since they are derived from the same dynamical system.

Similarly, more blocks can be treated in this way; here the third block is first projected orthogonally onto the subspace spanned by ϕ_1 and ϕ_2, then the complementary parts are used to do the POD analysis, and the eigenmodes for the complementary subspace for the third block can be obtained

$$\boldsymbol{W}_3 = \boldsymbol{U}_3 - \phi_1 \phi_1^T \boldsymbol{U}_3 - \phi_2 \phi_2^T \boldsymbol{U}_3 \tag{28}$$

while the POD analysis gives the eigenmodes of $\boldsymbol{W}_3$, which can be used to construct the approximation as follows:

$$\boldsymbol{W}_3 = \sum_{i=1}^{N_3} C_3^i \phi_3^i = \phi_3 \boldsymbol{C}_3 \tag{29}$$

where N_3 is the number of eigenmodes used in the approximation. Similarly, the approximation to the third block $\boldsymbol{U}_3$ in this case can be achieved by the following formulation:

$$\boldsymbol{U}_3 = \phi_1 \phi_1^T \boldsymbol{U}_3 + \phi_2 \phi_2^T \boldsymbol{U}_3 + \phi_3 \boldsymbol{C}_3 \tag{30}$$

Taking all the blocks of snapshots simultaneously into account, the extended POD analysis can be formally represented in the following matrix form:

$$\boldsymbol{U} = \phi \boldsymbol{C} \tag{31}$$

where

$$\boldsymbol{U} = [\boldsymbol{U}_1 \ \ \boldsymbol{U}_2 \ \ \boldsymbol{U}_3], \quad \phi = [\phi_1 \ \ \phi_2 \ \ \phi_3] \tag{32}$$

is a collection of snapshots and eigenmodes from each block, while the coefficient matrix is given as follows [83]:

$$\boldsymbol{C} = \begin{bmatrix} \boldsymbol{C}_1 & \phi_1^T \boldsymbol{U}_2 & \phi_1^T \boldsymbol{U}_3 \\ 0 & \boldsymbol{C}_2 & \phi_2^T \boldsymbol{U}_3 \\ 0 & 0 & \boldsymbol{C}_3 \end{bmatrix} \tag{33}$$

where all the entries in the matrix can be obtained once the blocks of snapshots are provided.

It is easy to see that ϕ_1, ϕ_2, and ϕ_3 are orthogonal to each other, which means that the Galerkin projection method will be exactly the same as we discussed in Sec. 3, when the extended POD analysis is employed to construct the basis functions with more than one block of snapshots. It is also easy to see that the approximations given by Eqs. (24), (27), and (30) are all satisfied by Eq. (33). For the case where more snapshot blocks are available, the extended POD can be carried out similarly.

It is worth noting that the choice of the number of eigenmodes for each block should be made on the basis of a compromise to balance the approximation error in each block, as discussed in Ref. [83]. In other words, the values for N_1, N_2, and N_3 should be chosen such that the approximation error in each block should be close. It is done based on numerical experiments for the current problem.

5 Numerical Results

A typical example of ferroelastic materials is provided by shape memory alloys (SMAs). Here, we demonstrate the feasibility of constructing a low dimensional model using the extended POD methods for the dynamics of SMAs involving mechanically and thermally-induced phase transformations. We analyze the performance of the low dimensional model by numerical experiments. The dynamics of a SMA rod is first simulated by using the PDE model, and the eigenmodes of the dynamics are extracted out from the numerical results. Then, the phase transformations induced by either mechanical or thermal loadings are simulated using the low dimensional model. The mechanical and thermal hystereses due to the martensitic phase transformation are also modeled using the developed low dimensional model.

5.1 POD Results. All the numerical experiments in the current section are performed on a $Au_{23}Cu_{30}Zn_{47}$ rod of length $L=1$ cm. All the numerical experiments are carried out with the same boundary conditions, as given by Eq. (5). All the physical parameters for this specific material are available in Ref. [36] and listed here for convenience

$$k_1 = 4.80 \times 10^7 \ \text{kg/s}^2\,\text{m K}, \quad k_2 = 6 \times 10^{11} \ \text{kg/s}^2\,\text{m K},$$

$$k_3 = 4.5 \times 10^{13} \ \text{kg/s}^2\,\text{m K}$$

$$\theta_1 = 208 \ \text{K}, \quad \rho = 1110 \ \text{kg/m}^3, \quad c_v = 2.9 \times 10^6 \ \text{kg/s}^2\,\text{m K},$$

$$k = 1.9 \times 10^2 \ \text{m kg/s}^3\,\text{K}$$

For the collections of snapshots, three representative numerical experiments are carried out first using the Chebyshev collocation method for the PDE model given by Eq. (2). In the computation, there are 15 nodes used for the Chebyshev approximation, the simulated time range is $t \in [0,24]$ ms, which corresponds to two loading periods, and the time step-size is set to 1×10^{-3} ms. For

each computation, there are 200 snapshots of the system states collected in the block.

The first experiment is expected to be representative of the dynamics of SMA at low temperature. The snapshot block $\boldsymbol{U}_1$ is collected with the following input:

$$F = 1 \times 10^9 \ \text{kg/s}^2\,\text{m}^2,$$

$$G = 7 \times 10^7 \begin{cases} \dfrac{t}{3}, & t < 3 \\ \dfrac{6-t}{3}, & t < 9 \\ \dfrac{12-t}{3}, & t < 12 \end{cases} \quad \text{kg/s}^2\,\text{m}$$

with the initial conditions: $v=0$, $\theta=210$ K, and $\varepsilon=0.01187 \times \text{sign}(x-0.5)$. This numerical experiment involves thermally-induced transformation [28,36], and it can be regarded as a representative case for thermally-induced transformations.

The second numerical experiment with the PDE model is carried out with the following initial conditions: $v=0$, $\theta=250$ K, and $\varepsilon=0$. At this given temperature, there are metastable phases in the SMA rod, and martensite and austenite might coexist under this temperature. The mechanical loading for this case is set to

$$G = 0, \quad F = \begin{cases} 7 \times 10^{10}, & 0 < t < 3 \\ 0, & 3 < t < 6 \\ -7000, & 6 < t < 9 \\ 0, & 9 < t < 12 \end{cases} \quad \text{kg/s}^2\,\text{m}^2$$

which is sufficient to induce phase transformations mechanically. The snapshot block $\boldsymbol{U}_2$ is collected through this experiment.

The third block of snapshots $\boldsymbol{U}_3$ is collected using the numerical experiment with mechanical loading at high initial temperature, in which case there is no phase transformation to be induced. The initial temperature is set to $\theta=310$ K, and the mechanical loading is chosen the same as in the second experiment ($v=0$, $\varepsilon=0$).

Both mechanically and thermally-induced phase transformations in SMA rods have been simulated using the same methodology discussed in Refs. [28,36,56], so the numerical results will not be presented here. Instead, we note the following. By employing the extended POD method, as discussed in Sec. 4, the eigenmodes for the dynamics of the SMA rod can be extracted from the three blocks of snapshots. Ideally, the POD analysis should be carried out in a vector-valued modes, as done in Ref. [84], since physical fields are coupled with each other dynamically. This strategy, however, is not followed here due to the fact that the magnitude of physical variables is very different for the current problem (e.g., three orders of magnitude differences in the strain and temperature distributions). A vector-valued POD analysis certainly will lead the resultant eigenmodes to have more influence from the characteristics of temperature distributions, while the mechanical characteristics will be almost ignored due to their rather small magnitudes compared with the thermal field. As we pointed out in Ref. [10], we deal here with a multiscale coupled problem, but in the first approximation in what follows the POD analysis is carried out separately for ε, v, and θ. This treatment will introduce an additional error to the low dimensional model, but as demonstrated below, the proposed approximation is capable of capturing the essential features of hysteretic dynamics and thermomechanical coupling as required in the low dimensional reduction.

To show the characteristics of the strain and temperature, the first three eigenmodes (associated with the largest eigenvalues) are plotted in Fig. 1, in which case the three eigenmodes for ε from the block $\boldsymbol{U}_1$ are in the left column and those for θ from U_1 are in the right column. There are in total four eigenmodes chosen from block $\boldsymbol{U}_1$ for each of ε, v, and θ.

For a better approximation to $\boldsymbol{U}_2$, there were two additional eigenmodes extracted and merged together with eigenmodes from $\boldsymbol{U}_1$. To clarify this, the first eigenmode for ε from $\boldsymbol{U}_2$ is plotted in Fig. 2(*a*), together with the first eigenmode for θ from $\boldsymbol{U}_2$ in Fig. 2(*b*). Only one additional eigenmode is extracted from $\boldsymbol{U}_3$. Therefore, for each variable, there are in total seven eigenmodes. Using these eigenmodes, the system states at any given moment of time can be approximated as

$$\epsilon = \sum_{i=1}^{7} \varepsilon_i \phi_i^{\varepsilon}, \quad v = \sum_{i=1}^{7} v_i \phi_i^{v}, \quad \theta = \sum_{i=1}^{7} \theta_i \phi_i^{\theta} \tag{34}$$

In order to show the performance of the approximation using the extended eigenmodes, the approximation error of the second block of snapshots $\boldsymbol{U}_2$ using Eq. (34) is presented in the upper part of Fig. 3. The absolute difference between the snapshots itself and their projection onto the eigenmodes is calculated as follows:

$$e_{\varepsilon} = \varepsilon(x,t) - \phi_{\varepsilon}\phi_{\varepsilon}^T \varepsilon(x,t), \quad e_{\theta} = \theta(x,t) - \phi_{\theta}\phi_{\theta}^T \theta(x,t) \tag{35}$$

which is used to measure the approximation error. In the plot, we present the absolute difference for all the discretization nodes and all the sample time instances. It is shown that the magnitude of the approximation error is smaller than 10^{-13} for ε and smaller than 10^{-10} for θ, which is negligible for most practical applications. In order to compare the approximations for different numbers of eigenmodes, the approximation error with ten eigenmodes for each variable are also presented in the same figure. Out of the ten eigenmodes, six are extracted out from block $\boldsymbol{U}_1$, three from $\boldsymbol{U}_2$, and one from $\boldsymbol{U}_3$. It is shown that the approximation error is smaller, the approximation is slightly improved. By increasing the number of eigenmodes further, numerical experiments show that the approximation will also be improved accordingly and finally will be saturated, confirming the convergence of the proposed procedure.

5.2 Low Dimensional Model Results. By substituting the above approximation into Eq. (2), the system is converted into a set of ODEs in form of Eq. (21), with dimension of 21. A standard ODE integrator (ode23 in MATLAB) is applied to simulate the state evolution under various loadings. To validate the low dimensional model, both mechanically and thermally-induced phase transformations are simulated using the developed low dimensional model, along with the associated hysteresis effects.

Although we deal with a relatively small number of eigenmodes, the system is not obtainable in an explicit form. The underlying numerical representation is based on the nonlinear evolution of a combination of these eigenmodes, making its numerical approximation the most natural way to solve the problem. In this case, the analysis of low dimensional models based on (multiscale) bifurcation and stability of equilibrium branches becomes a challenging task. For some special cases and simplified models of shape memory alloys, such an analysis has been carried out by several authors, as we already mentioned above [78–81]. Low dimensional models based on center manifold reductions have been analyzed in Refs. [8,10,14,35–37]. The interested reader can consult these publications for further detail. In what follows our focus is on the efficient numerical treatment of hysteresis effects.

The first numerical experiment is to demonstrate the thermally-induced transformation with a slightly higher initial temperature. The initial conditions are set to $v=0$, $\theta=220$ K, $\varepsilon=0.01187 \times \text{sign}(x-0.5)$, the loading for this experiment is chosen as $F=1 \times 10^9$ kg/s^2 m^2, $G=7\times10^7$ kg/s^2 m, and the simulation span is chosen as $t \in [0,24]$ ms. The dynamic behavior of the SMA rod under similar conditions has been investigated in Refs. [28,36], with different methodologies. Figure 4 (top) demonstrates that the phase transformations are captured by the low dimensional model developed here (the strain, $\varepsilon(x,t)$, and temperature, $\theta(x,t)$, distri-

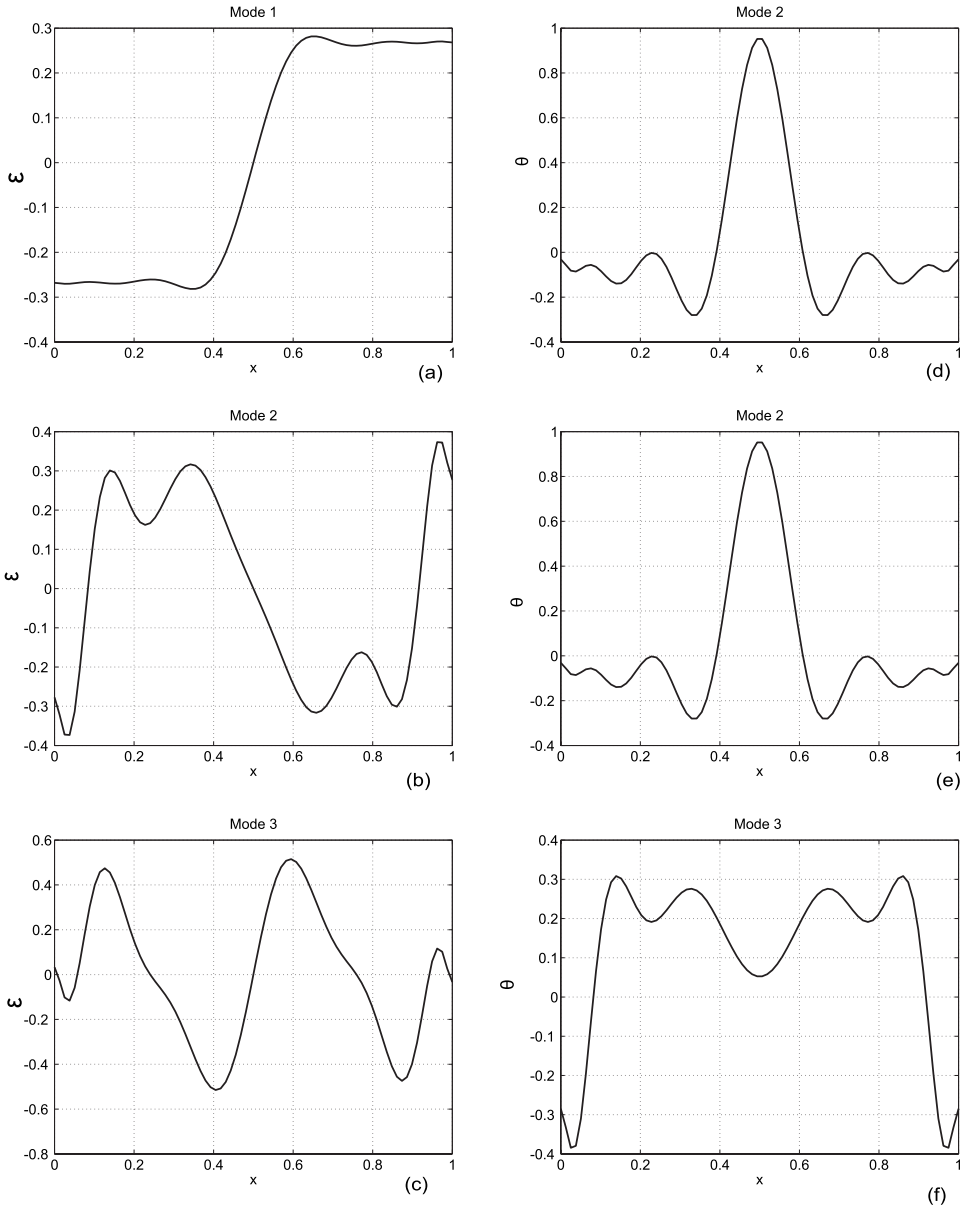

Fig. 1 The first three empirical eigenmodes for the strain distributions ((*a*), (*b*), and (*c*)) and temperature distributions ((*d*), (*e*), and (*f*))

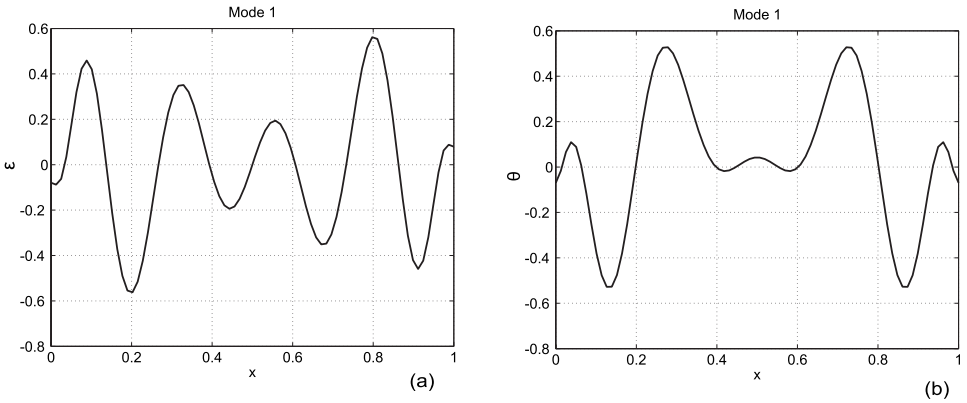

Fig. 2 The first empirical eigenmode for the strain distributions (*a*) and temperature distributions (*b*) in the second block of snapshots using the extended POD

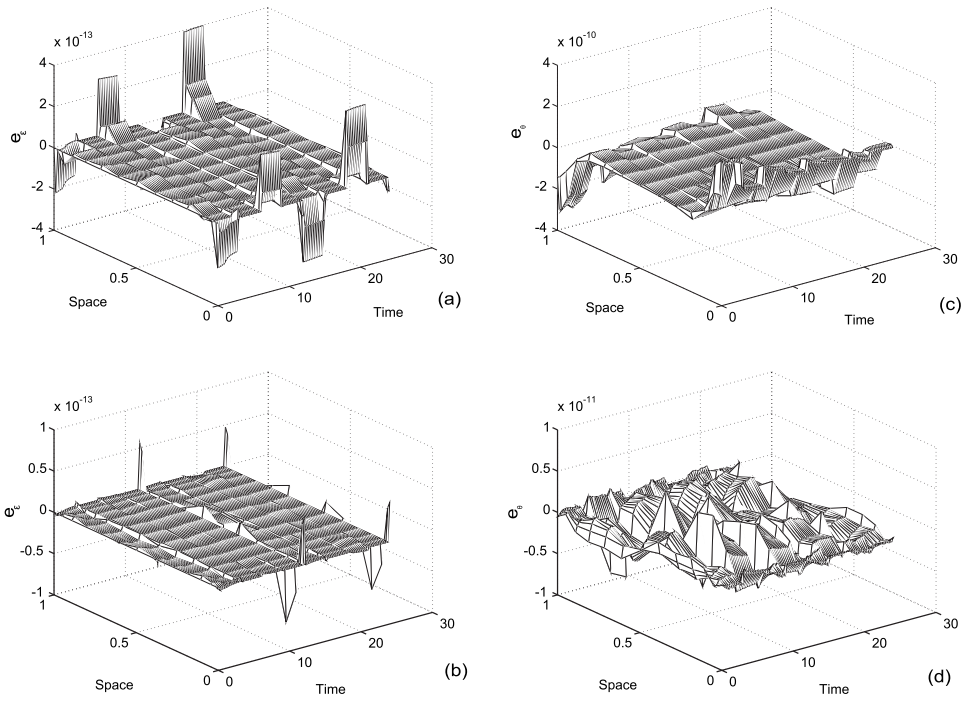

Fig. 3 The absolute approximation error to the second block of snapshots using different numbers of empirical eigenmodes: (a) seven modes for the strain distribution; (*b*) ten modes for the strain distribution; (*c*) seven modes for the temperature distribution; (*d*) ten modes for the temperature distribution

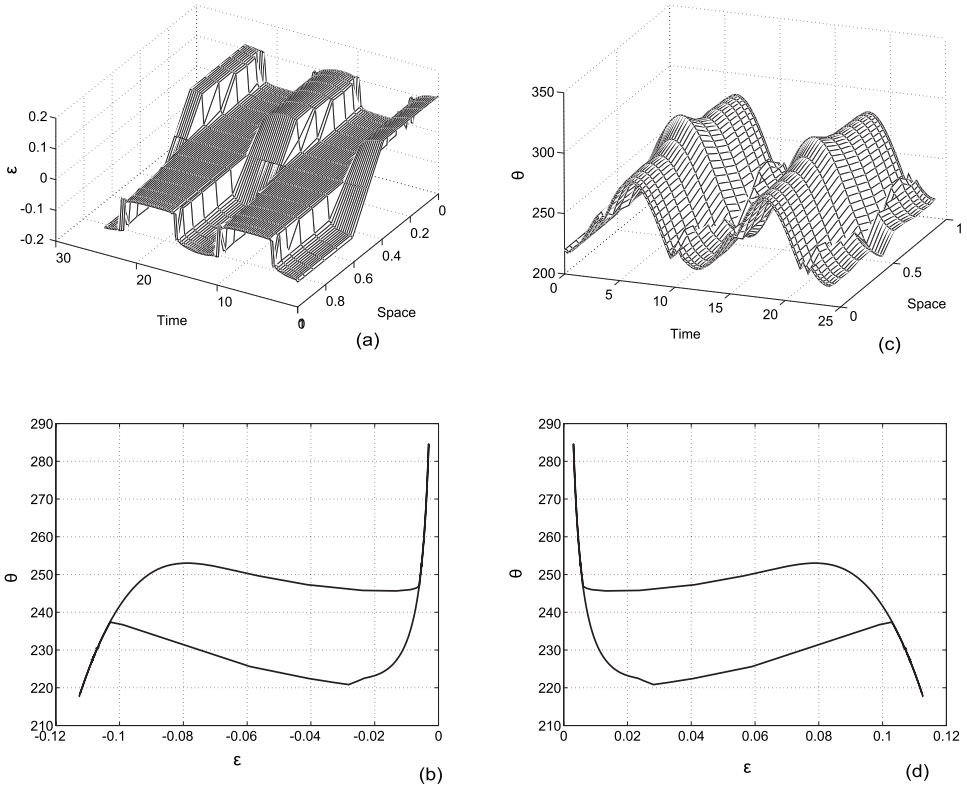

Fig. 4 Numerical results for thermally-induced phase transformations in a SMA rod obtained with the developed low dimensional model. (*a*) Strain distribution, (*b*) thermal hysteresis at $x = 0.1$ cm, (*c*) temperature distribution, and (*d*) thermal hysteresis at $x = 0.9$ cm.

butions are presented in subplots (a) and (c), respectively). The thermally-induced phase transformations between austenite and martensite are captured when the SMA rod is heated up ($M \rightarrow A$) or cooled down ($A \rightarrow M$). A simple explanation of the overall shape of the temperature-strain curves in the case of thermally-induced hysteresis was first proposed in Ref. [35]. There is a temperature difference between the $M \rightarrow A$ and $A \rightarrow M$ transformations, which is the origin of the related thermal hysteresis. To show this (thermally-induced) hysteresis, $\varepsilon(x,t)$ is plotted versus $\theta(x,t)$ at $x=0.1$ cm (for the fourth discretization node)—see subplot (b) in Fig. 4. Due to symmetry, a similar plot is obtained at point $x=0.9$ cm, as shown in subplot (d) in Fig. 4.

Note that the approximation of the underlying multiscale behavior of the ferroelastic material by using a fifth order polynomial for stress-strain relationships (derived from the sixth order Landau–Ginzburg free energy function) results in a high sensitivity of the solution with respect to the speed of parameter variation and, therefore, in numerical calculations accompanying oscillations are expected, even away from the transition points. One of the possible ways to overcome this difficulty is to modify the original model by including a visco-elastic term or the Rayleigh dissipation term, as it has been done in our model (1) (and (2)), following the ideas of Wang and Melnik [24,61] (see also references therein). This term accounts for the internal friction accompanying the movement of the interfaces between different phases. In all numerical calculations presented here (Figs. 4–6) this term was accounted for.

Next, we demonstrate the efficiency of the developed low dimensional model for different initial temperatures. The second numerical experiment is carried out with the following initial conditions: $v=0$, $\varepsilon=0$, and $\theta=255$ K. The loadings are set to $G=0$ and $F=6000\times(\sin(t\pi/6))^3$. The numerical results are presented in Fig. 5, $\varepsilon(x,t)$ (a) and $\theta(x,t)$ (b). It is seen that the entire rod is divided roughly into two parts, one with positive values of ϵ and the other with negative values ϵ, following the variation in the mechanical loading. In this case, $\theta(x,t)$ is also driven to oscillate because of the thermal-mechanical coupling. The hysteresis due to the phase transformation is presented by plotting the $\varepsilon(x,t)$ versus F (or stress) at $x=0.1$ in subplot (c) in Fig. 5. Observe that there are two subhysteresis loops in the plot, which can be explained by the facts that the material has metastable phases under the current initial temperature [28,36].

Finally, the developed low dimensional model is employed to analyze the mechanical hysteresis in the case of mechanically induced phase transformations and to compare the numerical results with theoretical predictions (see Fig. 6). Three different initial temperatures are chosen for the simulation. Because austenite is unstable when $\theta=220$ deg, the mechanical loading will switch the material between martensites plus and minus, as indicated by the constitutive curve plotted in subplot (a) in Fig. 6 (the transformation is $M+ \rightarrow M-$ or $M- \rightarrow M+$). In this case there is only one hysteresis loop which is sketched by the dashed line. The numerical simulation with this initial temperature (d) agrees well with this prediction. When the initial temperature of the material is increased to $\theta=240$ deg, the constitutive curve is plotted in subplot (b), where we observe two separated hysteresis loops due to metastable phases. The numerical results plotted in subplot (e) of this figure demonstrate that the two hysteresis loops are successfully simulated. If the initial temperature is increased further to $\theta=320$ deg, the constitutive curve (c) indicates that there is no phase transformation because only austenite is stable. In this case, there is no hysteresis loop as confirmed by the numerical results presented in subplot (f) in Fig. 6.

The numerical experiments demonstrated that the low dimensional model constructed using the extended POD method is capable of capturing the essential dynamics of the SMA rod under various mechanical and thermal loadings and a range of initial temperatures. Compared with the single parameter POD methods,

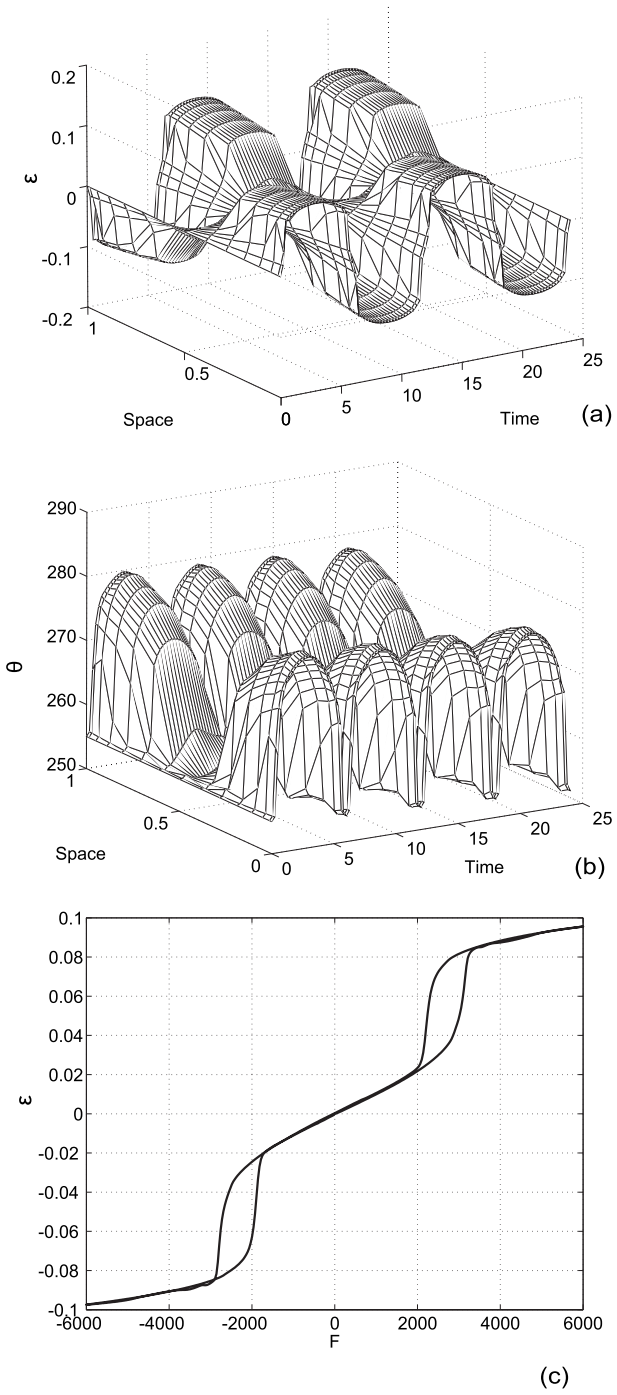

Fig. 5 Numerical results for a SMA rod obtained with the developed low dimensional model. (*a*) Strain distribution, (*b*) temperature distribution, and (*c*) mechanical hysteresis with $\theta=255$ deg.

the developed here extended POD-based low dimensional model covers the dynamics of the materials with full mechanical and thermal work range, which is essential for most of the engineering applications.

6 Conclusion

In the present paper, the dynamics of ferroelastic materials has been successfully simulated with a low dimensional model developed here on the basis of the extended POD. It has allowed us to model mechanically and thermally-induced transformations on the

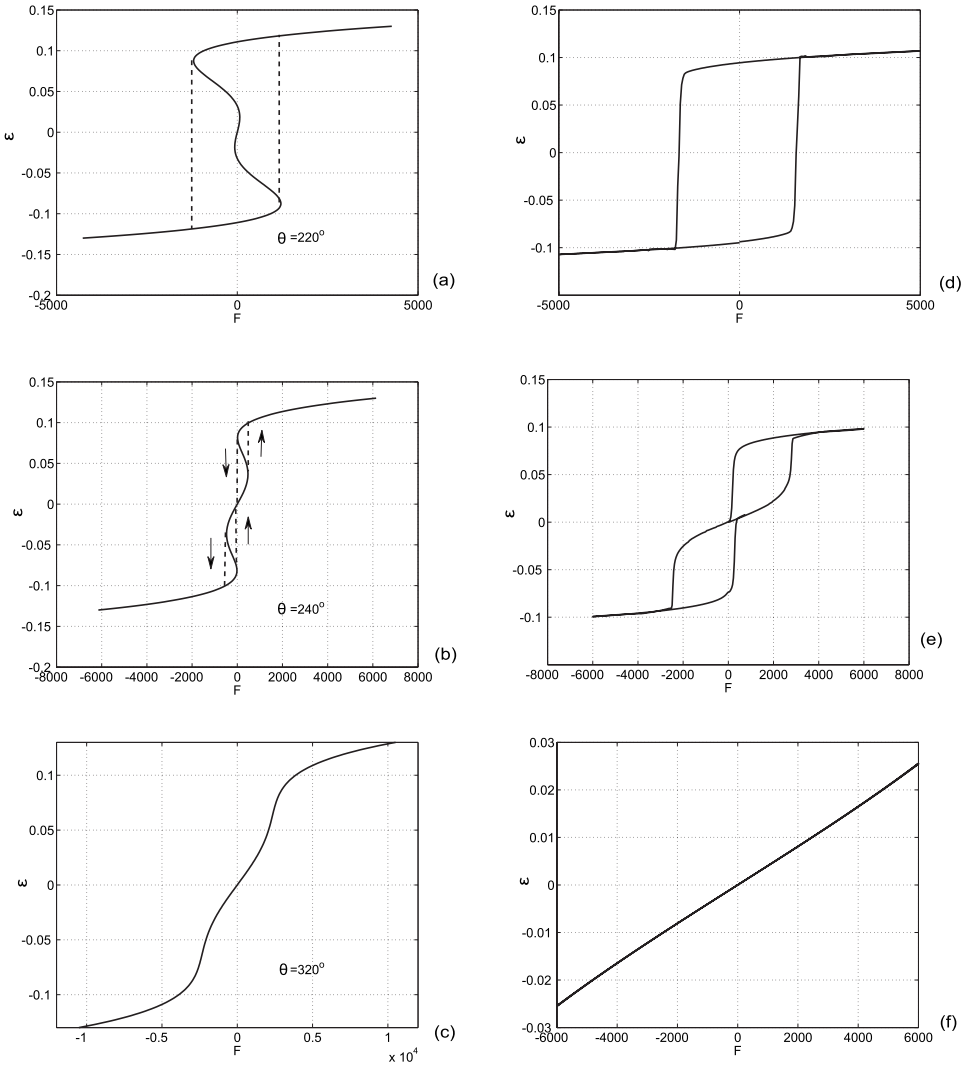

Fig. 6 Comparison of hysteretic behavior due to mechanically induced phase transformations: theoretical analysis ((*a*), (*b*), and (*c*)) and numerical simulation ((*d*), (*e*), and (*f*)); θ = 220 deg ((*a*) and (*d*)), θ=240 deg ((*b*) and (*e*)), θ=320 deg ((*c*) and (*f*))

example of shape memory alloy rod. First, the dynamics has been analyzed numerically by using a PDE model, and the appropriate collections of snapshots of the system states have been constructed during the simulation. Next, by using the extended proper orthogonal decomposition method, a set of common eigenmodes for the dynamics that covers the full temperature range has been obtained. Finally, the dynamics of the SMA rod has been projected orthogonally onto the subspace spanned by a small number of eigenmodes, and a low dimensional model has been derived. Numerical experiments have demonstrated that the dynamics of the SMA rod can be successfully captured by the developed low dimensional model. Both thermally and mechanically induced phase transformations and related hysteresis effects have been successfully reproduced with the constructed model.

Acknowledgment

The authors acknowledge the support of their funding agencies (L.W.—NNSF of China under Grant No. 10872062 and R.M.—the NSERC, the CRC program of Canada, and the Hans Christian Andersen Fellowship program of Denmark). Support of the Mads Clausen Foundation and useful comments by the referees are gratefully acknowledged by both of the authors.

References

[1] Wang, L. X., and Melnik, R. V. N., 2009, "Control of Coupled Hysteretic Dynamics of Ferroelectric Materials With a Landau-Type Differential Model and Feedback Linearization," Smart Mater. Struct., **18**(7), p. 074011.
[2] Banks, H. T., Smith, R. C., and Wang, Y., 1996, *Smart Material Structures: Modelling, Estimation and Control*, Wiley, Masson, Paris.
[3] Hu, M., Du, H., and Ling, S. F., 2000, "Motion Control of an Electrostrictive Actuator," Proc. SPIE, **4235**, pp. 321–327.
[4] Wang, L. X., and Melnik, R. V. N., 2007, "Model Reduction Applied to Square to Rectangular Martensitic Transformations Using Proper Orthogonal Decomposition," Appl. Numer. Math., **57**(5–7), pp. 510–520.
[5] Melnik, R. V. N., 1997, "The Stability Condition and Energy Estimate for Nonstationary Problems of Coupled Electroelasticity," Math. Mech. Solids, **2**(2), pp. 153–180.
[6] Melnik, R. V. N., and Melnik, K. N., 2000, "Modelling Dynamics of Piezoelectric Solids in the Two-Dimensional Case," Appl. Math. Model., **24**(3), pp. 147–163.
[7] Melnik, R. V. N., 2001, "Computational Analysis of Coupled Physical Fields in Piezothermoelastic Media," Comput. Phys. Commun., **142**(1–3), pp. 231–237.
[8] Melnik, R. V. N., and Roberts, A. J., 2002, "Computational Models for Materials With Shape Memory: Towards a Systematic Description of Coupled Phenomena," *Computational Science—ICCS 2002, PT II* (Lecture Notes in Computer Science), Vol. 2330, Springer, Amsterdam, pp. 490–499.
[9] Melnik, R. V. N., 2003, "Modelling Coupled Dynamics: Piezoelectric Elements Under Changing Temperature Conditions," Int. Commun. Heat Mass Transfer, **30**(1), pp. 83–92.
[10] Melnik, R. V. N., and Roberts, A., 2004, "Computational Models for Multi-

Scale Coupled Dynamic Problems," FGCS, Future Gener. Comput. Syst., **20**(3), pp. 453–464.
[11] Yang, X. D., and Melnik, R. V. N., 2009, "Effect of Internal Viscosity of Polymeric Fluids Under Strong Extensional Flows," Chin. J. Polym. Sci., **27**(2), pp. 189–193.
[12] Melnik, R. V. N., and Povitsky, A., 2004, "Wave Phenomena in Physics and Engineering: New Models, Algorithms, and Applications," Math. Comput. Simul., **65**(4–5), pp. 299–302.
[13] Kamath, H., Willatzen, M., and Melnik, R. V. N., 2006, "Vibration of Piezoelectric Elements Surrounded by Fluid Media," Ultrasonics, **44**(1), pp. 64–72.
[14] Melnik, R. V. N., Roberts, A. J., and Thomas, K. A., 2000, "Computing Dynamics of Copper-Based SMA Via Centre Manifold Reduction of 3D Models," Comput. Mater. Sci., **18**(3–4), pp. 255–268.
[15] Melnik, R. V. N., and Roberts, A. J., 2001, "Thermomechanical Behaviour of Thermoelectric SMA Actuators," J. Phys. IV, **11**, pp. Pr8-515–Pr8-520.
[16] Mahapatra, D. R., and Melnik, R., 2005, "Three-Dimensional Mathematical Models of Phase Transformation Kinetics in Shape Memory Alloys," Dynamics of Continuous Discrete and Impulsive Systems Series B-Applications & Algorithms, **2**, pp. 557–562.
[17] Wang, L., and Melnik, R., 2006, "Dynamics of Shape Memory Alloys Patches With Mechanically Induced Transformations," Discrete Contin. Dyn. Syst., **15**(4), pp. 1237–1252.
[18] Mahapatra, D. R., and Melnik, R. V. N., 2006, "Numerical Simulation of Phase Transformations in Shape Memory Alloy Thin Films," *Computational Science-ICCS 2006*, Vol. 3992, pp. 114–121.
[19] Wang, L. X., and Melnik, R. V. N., 2006, "Two-Dimensional Analysis of Shape Memory Alloys Under Small Loadings," Int. J. Multiscale Comp. Eng., **4**(2), pp. 291–304.
[20] Mahapatra, D. R., and Melnik, R. V. N., 2006, "Finite Element Analysis of Phase Transformation Dynamics in Shape Memory Alloys With a Consistent Landau-Ginzburg Free Energy Model," Mech. Adv. Mater. Structures, **13**(6), pp. 443–455.
[21] Wang, L. X., and Melnik, R. V. N., 2006, "Differential-Algebraic Approach to Coupled Problems of Dynamic Thermoelasticity," Appl. Math. Mech., **27**(9), pp. 1185–1196.
[22] Mahapatra, D. R., and Melnik, R. V. N., 2007, "Finite Element Modelling and Simulation of Phase Transformations in Shape Memory Alloy Thin Films," Int. J. Multiscale Comp. Eng., **5**(1), pp. 65–71.
[23] Mahapatra, D. R., and Melnik, R. V. N., 2007, "Finite Element Approach to Modelling Evolution of 3D Shape Memory Materials," Math. Comput. Simul., **76**(1–3), pp. 141–148.
[24] Wang, L. X., and Melnik, R. V. N., 2007, "Thermo-Mechanical Wave Propagations in Shape Memory Alloy Rod With Phase Transformations," Mech. Adv. Mater. Structures, **14**(8), pp. 665–676.
[25] Wang, L. X., and Melnik, R. V. N., 2008, "Simulation of Phase Combinations in Shape Memory Alloys Patches by Hybrid Optimization Methods," Appl. Numer. Math., **58**(4), pp. 511–524.
[26] Wang, L. X., and Melnik, R. V. N., 2008, "Modifying Macroscale Variant Combinations in a Two-Dimensional Structure Using Mechanical Loadings During Thermally Induced Transformation," Mater. Sci. Eng., A, **481-482**, pp. 190–193.
[27] Melnik, R. V. N., Wang, L., Matus, P., and Rybak, L., 2003, "Computational Aspects of Conservative Difference Schemes for Shape Memory Alloys Applications," Lect. Notes Comput. Sci., **2668**, pp. 791–800.
[28] Matus, P., Melnik, R., Wang, L., and Rybak, I., 2004, "Application of Fully Conservative Schemes in Nonlinear Thermoelasticity: Modelling Shape Memory Materials. Mathematics and Computers in Simulation," Math. Comput. Simul., **65**(4–5), pp. 489–509.
[29] Fattorini, H. O., 1999, *Infinite Dimensional Optimization and Control Theory*, Cambridge University Press, Cambridge, England.
[30] Teman, R., 1998, *Infinite Dimensional Dynamical Systems in Mechanics and Physics*, Springer-Verlag, New York.
[31] Melnik, R. V. N., and Jenkins, D. R., 2002, "On Computational Control of Flow in Airblast Atomisers for Pulmonary Drug Delivery," Int. J. Pharm., **239**(1–2), pp. 23–35.
[32] Wu, Z., Melnik, R. V. N., and Borup, F., 2007, "Model-Based Analysis and Simulation of Airflow Control Systems of Ventilation Units in Building Environments," Build. Environ., **42**(1), pp. 203–217.
[33] Melnik, R. V. N., 2003, "Deterministic and Stochastic Dynamics With Hyperbolic HJB-Type Equations," Dyn. Contin. Discrete Impulsive Syst.: Ser. A - Math. Anal., **10**(1–3), pp. 317–330.
[34] Melnik, R. V. N., 2008, "Markov Chain Network Training and Conservation Law Approximations: Linking Microscopic and Macroscopic Models for Evolution," Appl. Math. Comput., **199**(1), pp. 315–333.
[35] Melnik, R. V. N., Roberts, A. J., and Thomas, K. A., 2001, "Coupled Thermomechanical Dynamics of Phase Transformations in Shape Memory Alloys and Related Hysteresis Phenomena," Mech. Res. Commun., **28**(6), pp. 637–651.
[36] Melnik, R. V. N., Roberts, A. J., and Thomas, K. A., 2002, "Phase Transitions in Shape Memory Alloys With Hyperbolic Heat Conduction and Differential Algebraic Models," Comput. Mech., **29**(1), pp. 16–26.
[37] Melnik, R. V. N., and Robert, A. J., 2003, "Modelling Nonlinear Dynamics of Shape Memory Alloys With Approximate Models of Coupled Thermoelasticity," Z. Angew. Math. Mech., **83**(2), pp. 93–104.
[38] Wang, L. X., and Melnik, R. V. N., 2005, "Simulation of Nonlinear Thermomechanical Waves With an Empirical Low Dimensional Model," Lect. Notes Comput. Sci., **3514**, pp. 884–891.
[39] Holmes, P., Lumley, J. L., and Berkooz, G., 1996, *Turbulence, Coherent Structures, Dynamical Systems and Symmetry*, Cambridge University Press, Cambridge, England.
[40] Rowley, C. W., and Marsden, J. E., 2000, "Reconstruction Equations and Karhunen–Loève Expansions for Systems With Symmetry," Physica D, **142**, pp. 1–19.
[41] Falk, F., and Konopka, P., 1990, "Three-Dimensional Landau Theory Describing the Martensitic Phase Transformation of Shape Memory Alloys," J. Phys.: Condens. Matter, **2**, pp. 61–77.
[42] Melnik, R., and Mahapatra, R., 2007, "Coupled Effects in Quantum Dot Nanostructures With Nonlinear Strain and Bridging Modelling Scales," Comput. Struct., **85**(11–14), pp. 698–711.
[43] Melnik, R. V. N., 2001, "Discrete Models of Coupled Dynamic Thermoelasticity for Stress-Temperature Formulations," Appl. Math. Comput., **122**(1), pp. 107–132.
[44] Strunin, D. V., Melnik, R. V. N., and Roberts, A. J., 2001, "Coupled Thermomechanical Waves in Hyperbolic Thermoelasticity," J. Therm. Stresses, **24**(2), pp. 121–140.
[45] Melnik, R. V. N., Strunin, D. V., and Roberts, A. J., 2005, "Nonlinear Analysis of Rubber-Based Polymeric Materials With Thermal Relaxation Models," Numer. Heat Transfer, Part A, **47**(6), pp. 549–569.
[46] Wang, H., Dai, W., Nassar, R., and Melnik, R., 2006, "A Finite Difference Method For Studying Thermal Deformation in a Thin Film Exposed to Ultrashort-Pulsed Lasers," Int. J. Heat Mass Transfer, **49**(15–16), pp. 2712–2723.
[47] Wang, H. J., Dai, W., and Melnik, R., 2006, "A Finite Difference Method for Studying Thermal Deformation in a Double-Layered Thin Film Exposed to Ultrashort Pulsed Lasers," Int. J. Therm. Sci., **45**(12), pp. 1179–1196.
[48] Zhang, S. Y., Dai, W., Wang, H., and Melnik, R. V. N.2008, "A Finite Difference Method for Studying Thermal Deformation in a 3D Thin Film Exposed to Ultrashort Pulsed Lasers," Int. J. Heat Mass Transfer, **51**(7–8), pp. 1979–1995.
[49] Lassen, B., Willatzen, M., Melnik, R., and Lew Yan Voon, L. C., 2005, "A General Treatment of Deformation Effects in Hamiltonians for Inhomogeneous Crystalline Materials," J. Math. Phys., **46**(11), pp. 112102.
[50] Kournytskyi, T., Melnik, R. V. N., and Gachkevich, A., 2005, "Thermal Behavior of Absorbing and Scattering Glass Media Containing Molecular Water Impurity," Int. J. Therm. Sci., **44**(2), pp. 107–114.
[51] Melnik, R. V. N., and Povitsky, A., 2006, "A Special Issue on Modelling Coupled and Transport Phenomena in Nanotechnology," J. Comput. Theor. Nanosci., **3**(4), pp. i–ii.
[52] Patil, S. R., and Melnik, R. V. N., 2009, "Thermopiezoelectric Effects on Optoelectronic Properties of CdTe/ZnTe Quantum Wires," Phys. Status Solidi A, **206**(5), pp. 960–964.
[53] Patil, S. R., and Melnik, R. V. N., 2009, "Coupled Electromechanical Effects in II-VI Group Finite Length Semiconductor Nanowires," J. Phys. D, **42**(14), p. 145113.
[54] Patil, S. R., and Melnik, R. V. N., 2009, "Thermoelectromechanical Effects in Quantum Dots," Nanotechnology, **20**(12), p. 125402.
[55] Wang, L., Liu, R., and Melnik, R. V. N, 2009, "Modeling Large Reversible Electric-Field-Induced Strain in Ferroelectric Materials Using 90 Orientation Switching," Sci. China, Ser. E: Technol. Sci., **52**(1), pp. 141–147.
[56] Bubner, N., 1996, "Landau-Ginzburg Model for a Deformation-Driven Experiment on Shape Memory Alloys," Continuum Mech. Thermodyn., **8**, pp. 293–308.
[57] Mahapatra, D. R., and Melnik, R., 2005, "A Dynamic Model for Phase Transformations in 3D Samples of Shape Memory Alloys," *Computational Science-ICCS 2005, Pt 3* (Lecture Series in Computer Science), Vol. 3516, pp. 25–32.
[58] Wang, L. X., and Melnik, R. V. N., 2004, "Dynamics of Shape Memory Alloys Patches," Mater. Sci. Eng., A, **378**(1–2), pp. 470–474.
[59] Wang, L. X., and Melnik, R. V. N., 2007, "Finite Volume Analysis of Nonlinear Thermo-Mechanical Dynamics of Shape Memory Alloys," Heat Mass Transfer, **43**(6), pp. 535–546.
[60] Wang, L. X., and Melnik, R. V. N., 2006, "Mechanically Induced Phase Combination in Shape Memory Alloys by Chebyshev Collocation Methods," Mater. Sci. Eng., A, **438-440**, pp. 427–430.
[61] Wang, L. X., and Melnik, R. V. N., 2007, "Numerical Model for Vibration Damping Resulting From the First-Order Phase Transformations," Appl. Math. Model., **31**(9), pp. 2008–2018.
[62] Yang, X. D., and Melnik, R. V. N., 2007, "Effect of Internal Viscosity on Brownian Dynamics of DNA Molecules in Shear Flow," Comput. Biol. Chem., **31**(2), pp. 110–114.
[63] Melnik, R. V. N., and Melnik, K. N., 1998, "A Note on the Class of Weakly Coupled Problems of Non-Stationary Piezoelectricity," Commun. Numer. Methods Eng., **14**(9), pp. 839–847.
[64] Melnik, R. V. N., 1998, "Convergence of the Operator-Difference Scheme to Generalized Solutions of a Coupled Field Theory Problem," Journal of Difference Equations and Applications, **4**(2), pp. 185–212.
[65] Melnik, R. V. N., 2000, "Generalised Solutions, Discrete Models and Energy Estimates for a 2D Problem of Coupled Field Theory," Appl. Math. Comput., **107**(1), pp. 27–55.
[66] Melnik, R. V. N., 2003, "Numerical Analysis of Dynamic Characteristics of Coupled Piezoelectric Systems in Acoustic Media," Math. Comput. Simul., **61**(3–6), pp. 497–507.
[67] Willatzen, M., Melnik, R. V. N., Galeriu, C., and Lew Yan Voon, L. C., 2003, "Finite Element Analysis of Nanowire Superlattice Structures," Lect. Notes Comput. Sci., **2668**, pp. 755–763.

[68] Melnik, R. V. N., 2009, "Coupling Control and Human Factors in Mathematical Models of Complex Systems," Eng. Applic. Artif. Intell., **22**(3), pp. 351–362.
[69] Melnik, R. V. N., and Zotsenko, K. N., 2004, "Mixed Electroelastic Waves and CFL Stability Conditions in Computational Piezoelectricity," Appl. Numer. Math., **48**(1), pp. 41–62.
[70] Trefethen, L. N., 2000, *Spectral Method in Matlab*, SIAM, Philadelphia, PA.
[71] Liang, Y. C., Lee, H. P., Lim, S. P., Lin, W. Z., Lee, K. H., and Wu, C. G., 2002, "Proper Orthogonal Decomposition and Its Applications—Part I: Theory," J. Sound Vib., **252**(3), pp. 527–544.
[72] Melnik, K. N., and Melnik, R. V. N., 1999, "Optimal-by-Order Quadrature Formulae for Fast Oscillatory Functions With Inaccurately Given A Priori Information," J. Comput. Appl. Math., **110**(1), pp. 45–72.
[73] Melnik, K. N., and Melnik, R. V. N., 2001, "Optimal Cubature Formulae and Recovery of Fast-Oscillating Functions From an Interpolational Class," BIT, **41**(4), pp. 748–775.
[74] Melnik, R. V. N., 2000, "Topological Analysis of Eigenvalues in Engineering Computations," Eng. Comput., **17**(4), pp. 386–416.
[75] Melnik, K. N., and Melnik, R. V. N., 2002, "Optimal-by-Accuracy and Optimal-by-Order Cubature Formulae in Interpolational Classes," J. Comput. Appl. Math., **147**(1), pp. 233–262.
[76] Zotsenko, K. N., and Melnik, R. V. N., 2004, "Optimal Minimax Algorithm for Integrating Fast Oscillatory Functions in Two Dimensions," Eng. Comput., **21**(8), pp. 834–847.
[77] Kerschen, G., and Colinval, J. C., 2002, "Physical Interpretation of the Proper Orthogonal Modes Using the Singular Value Decomposition," J. Sound Vib., **249**(5), pp. 849–865.
[78] Machado, L. G., Savi, M. A., and Pacheco, M. C. L., 2004, "Bifurcations and Crises in a Shape Memory Oscillator," Shock Vib., **11**, pp. 67–80.
[79] Lacarbonara, W., Bernardini, D., and Vestroni, F., 2004, "Nonlinear Thermomechanical Oscillations of Shape-Memory Devices," Int. J. Solids Struct., **41**, pp. 1209–1234.
[80] Bernardini, D., and Rega, G., 2005, "Thermomechanical Modelling, Nonlinear Dynamics and Chaos in Shape Memory Oscillators," Math. Comput. Model. Dyn. Syst., **11**(3), pp. 291–314.
[81] Elliott, R. S., 2007, "Multiscale Bifurcation and Stability of Multilattices," J. Comput.-Aided Mater. Des., **14**, pp. 143–157.
[82] Bui-Thanh, T., Damodaran, M., and Willcox, K., 2003, "Proper Orthogonal Decomposition Extensions for Parametric Applications in Transonic Aerodynamics," AIAA Paper No. 2003-4213.
[83] Jørgensen, B. H., Sørensen, J. N., and Brøns, M., 2003, "Low-Dimensional Modelling of a Driven Cavity Flow With Two Free Parameters," Theor. Comput. Fluid Dyn., **16**, pp. 299–317.
[84] Rowley, C. W., Colonius, T., and Murray, R. M., 2004, "Model Reduction for Compressible Flows Using POD and Galerkin Projection," Physica D, **189**, pp. 115–129.